



ORIGINAL ARTICLE

Mechanistic and kinetic insights into size-dependent activity in ultra-small Pt/CNTs nanozymes during antibacterial process



Jie Yang^a, Xiaofeng Ren^a, Xiaoyu Zhang^a, Xiaozhe Wang^a, Rong Zhang^a,
Peirong Bai^a, Baojie Du^a, Liping Li^{a,*}, Shichao Zhao^{b,*}, Yong Qin^{b,*},
Ruiping Zhang^{c,*}

^a Third Hospital of Shanxi Medical University, Shanxi Bethune Hospital, Shanxi Academy of Medical Sciences, Taiyuan 030032, China

^b State Key Laboratory of Coal Conversion, Institute of Coal Chemistry, Chinese Academy of Sciences, Taiyuan 030001, China

^c The Radiology Department of First Hospital of Shanxi Medical University, Taiyuan 030001, China

Received 30 June 2022; accepted 4 September 2022

Available online 9 September 2022

KEYWORDS

Size-dependent activity;
Nanozyme;
Atomic layer deposition;
Mechanism;
Kinetic

Abstract In enzyme-like catalytic reactions, the size effect of nanoparticles has been an essential yet unclear factor for the catalytic activity of nanozymes. Moreover, the synthesis of nanozymes with controllable size and electronic structures represents a grand challenge, which limits the systemic exploration the underlying nature of their structure–property relations and practical application. In this work, we proposed a novel strategy to regulate the size of Pt (0.55 ~ 2.81 nm) by atomic layer deposition for precisely tailoring Pt-based nanozymes. The size-dependent electronic and kinetic effects have been observed for the peroxidase-like reaction and antibacterial process, revealing a volcano-type dependence of intrinsic activity on Pt nanoparticle sizes, and the optimum Pt nanoparticle size was found to be ca. 1.69 nm. A combination of kinetic study and XPS analyses, as well as multiple nanozyme characterizations, demonstrates that Pt nanoparticles with an appropriate size contribute to proper affinity to the substrates, relating to a high ratio of Pt⁰/Pt²⁺ on the surface of Pt nanoparticles, which is beneficial to obtain the excellent catalytic performance and

* Corresponding authors.

E-mail addresses: liliping_8103@163.com (L. Li), zhaoshichao@sxicc.ac.cn (S. Zhao), qinyong@sxicc.ac.cn (Y. Qin), zrp_7142@sxmu.edu.cn (R. Zhang).

Peer review under responsibility of King Saud University.



antibacterial activity. Our work provides insights for an in-depth understanding size-dependent catalytic mechanism of nanozymes during antibacterial processes.

© 2022 The Author(s). Published by Elsevier B.V. on behalf of King Saud University. This is an open access article under the CC BY license (<http://creativecommons.org/licenses/by/4.0/>).

1. Introduction

Nanozyme is nanomaterial with intrinsic enzyme-like performance, has received increasing attention due to the advantages of tunable catalytic activity, high stability and low cost. (Liang and Yan, 2019; Jiang et al., 2019; Wang et al., 2019) The intrinsic properties of nanozymes are highly dependent on their physicochemical parameters including size, shape, composition, surface modification, and surrounding environments. As the most important parameter affecting the activity of nanozymes, many studies have demonstrated nanozymes including metals or non-metals, metal oxides, and alloy, have the size-dependent activity. (Bell and Alexis, 2003; Chen et al., 2007; Li and Xia, 2010; Sanchez et al., 1999; Wang et al., 2020; Li et al., 2020) Theoretically, nanozymes with smaller size are of higher catalytic activity than the larger ones due to greater specific surface areas and higher atomic utilization. However, this may not be the case. Geometrically, as the particle size decreases, the low-coordination atoms are gradually exposed and the proportion gradually increases, which significantly changes the structure and proportion of the active centers of the nanozymes. From the electronic structure point of view, the electronic energy levels of the particles are also significantly changed due to the quantum size effect, which greatly affects the orbital hybridization and charge transfer between the nanozymes and substrates. (Wilson et al., 2006; Mayrhofer et al., 2005; den Breejen et al., 2009; Wang et al., 2019) This strong entanglement of the geometric and electronic properties with the particle size makes identification of their distinct size-dependent properties nearly impossible. Furthermore, the kinetic behavior of catalysts is also an essential factor. Therefore, it is highly desirable to explore the main factors affecting nanozyme activity, and an in-depth understanding of the mechanism of size-dependent activity has far-reaching implications for the *de novo* design of nanozymes.

Nevertheless, as far as we know, a deep understanding of size-dependent activity in nanozyme has rarely been reported so far, especially for the ultra-small size of nanozymes. The main difficulty of in-depth interpretation of the size-dependent mechanisms might be attributed to the fact that traditional methods can not accurately control the size and geometry of nanozymes and have a large size distribution, (Moglietti et al., 2016) making it hard to accurately study the mechanisms by which electrons, geometries, and kinetic behavior vary with size. Atomic layer deposition (ALD) is considered to be an ideal method to precisely construct nanocatalysts with tunable size at atomic scale due to its self-limiting and the ample scope of materials that can be deposited. (Zhang and Qin, 2018; Zhao et al., 2021; Zhang et al., 2020) Our previous work reported the atomic-level precise synthesis of Pt/graphene sub-nanocatalysts (from single atom and dimer to cluster) by a high-temperature pulsed ozone strategy of ALD. (Yang et al., 2021) Furthermore, Chen et al. reported that the interface structure of nanozymes could also be precisely engineered by ALD to adjust their enzyme-mimicking activities. (Chen et al., 2020) However, until now, there has been no report on investigating the size-dependent mechanisms of nanozymes by ALD.

Here, a series of carbon nanotube-supported ultra-small Pt-based nanozymes (Pt/CNTs, 0.55 ~ 2.81 nm) were synthesized by ALD. The size of Pt nanoparticles can be precisely controlled by adjusting the cycle number of ALD. Their size-dependent electronic and geometric effects as well as unique peroxidase (POD)-like activity have been systematically investigated. A volcano-type dependence of intrinsic antibacterial activity on the size of Pt nanozymes has been elaborated.

Our work demonstrates the feasibility of ALD in precisely regulating nanozymes and provides insights into the catalytic mechanism of nanozymes in terms of the electronic effect and kinetic analysis.

2. Experimental

2.1. Materials

Raw multi-walled carbon nanotubes (CNTs) with a diameter of 5–15 nm and a length of 0.5–2 μm were purchased from J&K Scientific Ltd. (China). Trimethyl(methylcyclopentadienyl)platinum (IV) (MeCpPtMe_3), dimethyl sulfoxide (DMSO), hydrogen peroxide (H_2O_2), 3,3',5,5'-Tetramethylbenzidine (TMB) and the other chemicals were all obtained from Sigma-Aldrich.

2.2. Synthesis of *cPt/CNTs* nanozymes

Firstly, the raw CNTs were pretreated with HNO_3 in a 110 $^\circ\text{C}$ oil bath for 4 h to remove amorphous carbon and open the CNTs ends, and then washed with deionized water until there was no further change in pH ($\text{pH} \approx 7$). After that, the samples were further washed with absolute ethanol and then filtered. Finally, the functionalized CNTs were dried overnight in an oven at 100 $^\circ\text{C}$.

Before ALD, the functionalized CNTs were dispersed in ethanol by ultrasonic stirring, dropped onto a quartz wafer, and dried in air. Pt nanoparticles were deposited onto CNTs using a hot-wall, closed-chamber ALD reactor and the prepared nanozymes were named *cPt/CNTs* ($c = 5, 10, 20, 30, 50$ and 70). Then, the size of Pt nanoparticles can be precisely controlled by tuning the cycle number (c) of Pt ALD. The deposition temperature for Pt was 270 $^\circ\text{C}$ and MeCpPtMe_3 was kept at 60 $^\circ\text{C}$. Nitrogen was used as carrier and purge gas.

2.3. Characterization

The XRD patterns were collected using a Bruker D8 Advance X-ray diffractometer, whose $\text{Cu K}\alpha$ radiation ($\lambda = 1.540 \text{ \AA}$) is in the 2θ range from 5° to 90° . Pt loading in all nanozymes was determined by an inductively coupled plasma atomic emission spectrometer (ICP-AES, Thermo ICAP 6300). Transmission electron microscopy (TEM) and high-resolution TEM (HRTEM) images were taken with a JEOL-2100F microscope. X-ray photoelectron spectroscopy (XPS) measurements were performed using a Thermo ESCALAB 250 xi, which uses $\text{Al-K}\alpha$ line as the radiation source.

2.4. POD-like activity assay

The POD-like activity of *cPt/CNTs* nanozymes (2 μmol of Pt) was characterized by oxidation of TMB (1 mM) in the presence of H_2O_2 (20 mM). The experiment was carried out in 0.2 M sodium acetate buffer (NaAc-HAc , $\text{pH} = 3.6$), and

the absorbance at 652 nm was measured with a spectrophotometer.

The POD-like activity of *cPt/CNTs* nanozymes was quantitatively characterized by the standard method established in the literature. (Jiang et al., 2018) In short, using 0.5 mM TMB as a colorimetric substrate, various amounts (5 to 30 $\mu\text{g/mL}$) of *cPt/CNTs* nanozymes were added at 37 °C with 40 mM H_2O_2 in 0.2 M NaAc-HAc buffer (pH = 3.6), and the colorimetric response at 652 nm was measured by absorbance every 10 s for up to 600 s. Plot the relationship between absorbance at 652 nm and reaction time to obtain a reaction-time curve. Calculate the specific activity (SA) using the following equation: $a_{\text{nanozyme}} = V/(\epsilon \times l) \times (\Delta A/\Delta t)/[n]$, where *a*_{nanozyme} is the SA expressed in units per mole (U mol^{-1}) of nanozyme; *V* is the total volume of reaction system (μL); ϵ is the molar absorption coefficient of TMB ($39000 \text{ M}^{-1}\text{cm}^{-1}$); *l* is the length of light propagation path in the cuvette (cm); *A* is the absorbance after subtracting the blank value; and $\Delta A/\Delta t$ is the initial change rate of absorbance at 652 nm min^{-1} ; [*n*] is the mole of Pt atom.

2.5. Detection of hydroxyl radical ($\bullet\text{OH}$)

The generation of $\bullet\text{OH}$ was evaluated by electron spin resonance (ESR) spectrometer using DMPO (5,5-dimethyl-1-pyrroline *N*-oxide) spin-trapping adduct. First, 0.1 mL of *cPt/CNTs* (*c* = 5, 10, 20, 30, 50, and 70) nanozymes were dispersed in pH 4.5 NaAc buffer (0.2 M). Then, 20 mM of DMPO and 1 ML H_2O_2 were added to the mixture solution, respectively. The mixture was reacted at room temperature and air for 10 min, the solutions were then aspirated into quartz capillaries for ESR analysis. (Meng et al., 2022).

2.6. Steady-state kinetic assay

The steady-state kinetic assay of *cPt/CNTs* nanozymes was determined at room temperature. (Jiang et al., 2018) 20 $\mu\text{g/mL}$ of nanozyme and 1 M H_2O_2 were added into 0.2 M NaAc-HAc buffer (pH = 3.6) and mix well, then various concentrations (0.2 to 1.7 mM) of TMB solution were added, and record the initial rate of change of absorbance at 652 nm. The rate of increase in absorbance was converted to the substrate concentration in micromoles per minute (that is, the catalytic reaction rate, *v*) and plotted against substrate concentration to generate a Michaelis-Menten curve. Kinetic constants v_{max} and K_{m} were calculated by fitting the reaction rate values and substrate concentrations to the Michaelis-Menten equation as follows: $v = (v_{\text{max}} \times [\text{S}])/(K_{\text{m}} + [\text{S}])$, where *v* is the initial reaction rate, v_{max} is the maximal reaction rate. [*S*] is the concentration of the substrate and K_{m} is the Michaelis constant. The catalytic constant (k_{cat}) was calculated using the following equation: $k_{\text{cat}} = v_{\text{max}}/[\text{E}]$, where k_{cat} is the rate constant, which defines the maximum number of substrate molecules converted into products per unit time. [*E*] is the nanozyme concentration (M).

2.7. Antibacterial effect of *Pt/CNTs* nanozymes

The antibacterial effect of the *Pt/CNTs* nanozymes was determined via the number of colony forming units (CFU) using the plate counting method. (Wei et al., 2021; Weng et al., 2022)

Antibacterial experiments were performed in PBS to evaluate the effect of *cPt/CNTs* nanozymes on gram-negative bacteria (*Escherichia coli*; *E. coli*) and gram-positive bacteria (*Staphylococcus aureus*, *S. aureus*). Add *cPt/CNTs* nanozymes and H_2O_2 (10 mM) to 1 mL bacterial suspension ($1 \times 10^6 \text{ CFU}\cdot\text{mL}^{-1}$). The final concentration of *cPt/CNTs* nanozymes and H_2O_2 is 200 $\mu\text{g}\cdot\text{mL}^{-1}$ and 0.2 mM, respectively. Then continue the incubation at 37 °C for 2 h. After dilution of the bacterial solution, take 100 μL and spread over the surface of the Luria-Bertani (LB) medium, after incubating at 37 °C for 24 h, measure the optical density of the suspension at 652 nm using a microplate reader (MXQ 200) and finally calculate the antibacterial rate.

The paper-disk diffusion method was further employed to assay the antibacterial activities of *cPt/CNTs* nanozymes on *E. coli* and *S. aureus*. (Xia et al., 2018; Yang et al., 2019) The medium used for growing and maintaining the bacterial liquid cultures was LB medium, and a solid medium was obtained by adding 2 % agar into the liquid medium. 100 μg of as-prepared samples were uniformly dispersed on the filter paper discs (0.5 cm in diameter). The diameters of the inhibition zones were measured after incubation at 37 °C for 24 h.

3. Results and discussion

3.1. Preparation and characterization

The schematic preparation process of *Pt/CNTs* nanozymes via ALD is displayed in Fig. 1A. The section diagram of the preparation process is shown in Figure S1. First of all, with CNTs as the support, a certain cycle number (*c*₁) of Pt is deposited on its surface by ALD and named *c*₁*Pt/CNTs* nanozyme. Then the size of Pt nanoparticles can be accurately controlled by tuning the cycle number (*c*₂) of Pt ALD, that is, *c*₂*Pt/CNTs* nanozyme. To characterize the morphology of the as-deposited *cPt/CNTs* (*c* = 5, 10, 20, 30, 50, and 70) nanozymes, TEM measurements were conducted, and the results are depicted in Fig. 1B-1G. For the sample of 5*Pt/CNTs*, the Pt nanoparticles on the surface of the CNTs are so small that they are barely visible (as shown in red circles), which is due to the relatively few cycles of Pt ALD, resulting in a lower load rate of Pt on its surface. As the cycle number of Pt ALD increases, the size of Pt nanoparticles gradually becomes larger and uniformly distribute on the surface of CNTs. The mean particle sizes over *cPt/CNTs* nanozymes were counted according to the TEM images to more clearly characterize the size of Pt nanoparticles. As shown in Figure S2, the mean particle sizes of the six nanozymes are 0.55 nm, 0.82 nm, 1.42 nm, 1.69 nm, 2.05 nm and 2.81 nm, respectively. The HRTEM image highlights the well-defined lattice spacing of $\sim 0.223 \text{ nm}$ for Pt nanoparticles (Figure S3A), corresponding to the Pt(111) planes. (Zhang et al., 2019; Ramachandran et al., 2016) Moreover, based on ICP-AES measurements, the Pt loadings of *cPt/CNTs* (*c* = 5, 10, 20, 30, 50, and 70) nanozymes are 0.19 wt%, 0.34 wt%, 1.27 wt%, 1.61 wt%, 2.75 wt%, and 3.92 wt%, respectively (Table S1). These results demonstrate the superiority of ALD and corroborate that ALD can be used as a novel way to precisely synthesize Pt-based nanozymes with ultrasmall and tunable size.

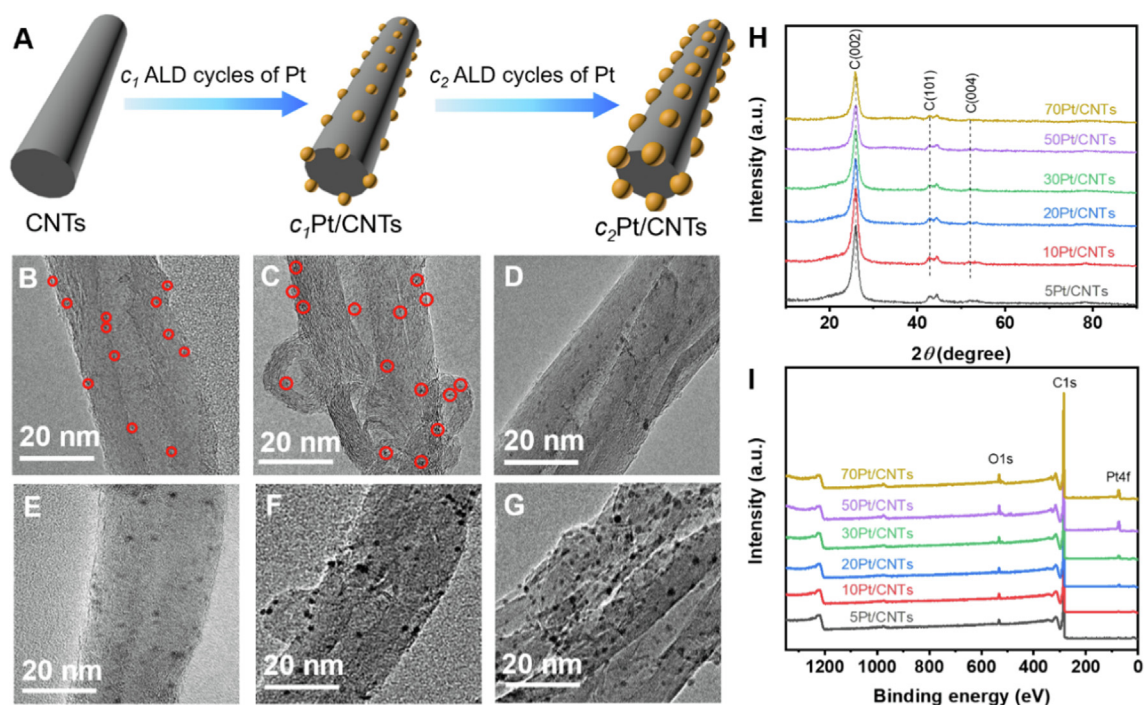


Fig. 1 Synthesis and structural characterizations of Pt/CNTs nanozymes. (A) Illustration of the preparation process of Pt/CNTs nanozymes. (B-G) TEM images of 5Pt/CNTs, 10Pt/CNTs, 20Pt/CNTs, 30Pt/CNTs, 50Pt/CNTs and 70Pt/CNTs, respectively. Note: red circles refer to Pt nanoparticles. (H, I) XRD patterns and XPS survey spectra of *c*Pt/CNTs nanozymes.

The X-ray diffraction (XRD) was further conducted to reveal the chemical structure of nanozymes, and the spectra of *c*Pt/CNTs are presented in Fig. 1H. The XRD patterns of 5Pt/CNTs, 10Pt/CNTs, 20Pt/CNTs, 30Pt/CNTs, 50Pt/CNTs and 70Pt/CNTs exhibit three strong diffraction peaks at around 25.9° , 42.8° , and 52.1° , which can be assigned to the C(002), C(101) and C(004) planes of the graphite structure of CNTs (PDF#75–1621), respectively. (Li et al., 2018; Xing et al., 2022) However, no characteristic peak of Pt could be observed, probably because its high dispersion and/or low content of Pt nanoparticles. Moreover, the XPS measurement was further conducted to investigate the surface elemental composition of *c*Pt/CNTs nanozymes. Fig. 1I shows the presence of carbon and oxygen atoms in the XPS survey spectra of all the *c*Pt/CNTs nanozymes. When the cycle number of Pt ALD is less than 10, no peak of Pt atom is observed in the XPS survey spectra. Still, the peak of Pt atom begins to appear when the cycle number of Pt ALD increases to 20, which may be due to the low content of Pt and/or the relatively high detection limit of XPS instruments, which is consistent with the above XRD results. The above results demonstrate that Pt/CNTs nanozymes are successfully prepared by ALD, and ALD can be used as a novel way to accurately synthesize ultra-small size and highly dispersed nanozymes.

3.2. Size-dependent POD-like activities of Pt/CNTs nanozymes

Pt nanoparticles with intrinsic POD-like catalytic activity have attracted significant interest due to their ability to replace specific POD enzymes in POD-based applications. (Liu et al., 2018; Ge et al., 2018; Chen et al., 2021) We evaluated the POD-like activities of the *c*Pt/CNTs nanozymes with different

sizes of Pt through the oxidation of 3,3',5,5'-tetramethylbenzidine (TMB, a typical POD substrate (Jiang et al., 2018) by H_2O_2 as a model catalytic reaction. As shown in Fig. 2A, the *c*Pt/CNTs nanozymes rapidly catalyzed the oxidation of TMB in the presence of H_2O_2 , producing a blue-colored oxidation product with an absorbance maximum at 652 nm. In contrast, bare CNTs, without Pt nanoparticles, alone did not lead to a color change. Moreover, the 30Pt/CNTs nanozyme has the highest catalytic activity of TMB oxidation by H_2O_2 in all *c*Pt/CNTs nanozymes. Then, we combined the absorbance values of the *c*Pt/CNTs nanozyme at 652 nm with the size of the Pt nanoparticles, as shown in Fig. 2B, it is found that the absorbance value at 652 nm of Pt nanozymes exhibits a volcanic relationship with the size of Pt nanoparticles. The Pt particles with a size of 1.69 nm (30Pt/CNTs nanozyme) present the highest absorbance value. The nanozyme activity standardization method was introduced to quantify the catalytic activities. The SA is defined as activity units (one nanozyme activity unit (U) is defined as the amount of nanozyme that catalytically produces $1 \mu\text{mol}$ of product per minute.) of per mole nanozyme. (Jiang et al., 2018) The reaction-time curves were obtained by plotting the absorbance at 652 nm against the reaction time (Figure S3B). As depicted in the inset of Figure S3B, for initial 60 s of the reaction, the nanozyme produces product at an initial rate that is approximately linear to the reaction time. The SA values of 5Pt/CNTs, 10Pt/CNTs, 20Pt/CNTs, 30Pt/CNTs, 50Pt/CNTs, and 70Pt/CNTs were calculated as $0.23 \text{ U } \mu\text{mol}^{-1}$, $1.03 \text{ U } \mu\text{mol}^{-1}$, $4.95 \text{ U } \mu\text{mol}^{-1}$, $5.58 \text{ U } \mu\text{mol}^{-1}$, $3.64 \text{ U } \mu\text{mol}^{-1}$, and $1.20 \text{ U } \mu\text{mol}^{-1}$, respectively, using the nanozyme activity standardization method (Figure S4 and Table S2). Then, plotting the SA values of the *c*Pt/CNTs nanozymes against the size of the Pt nanoparti-

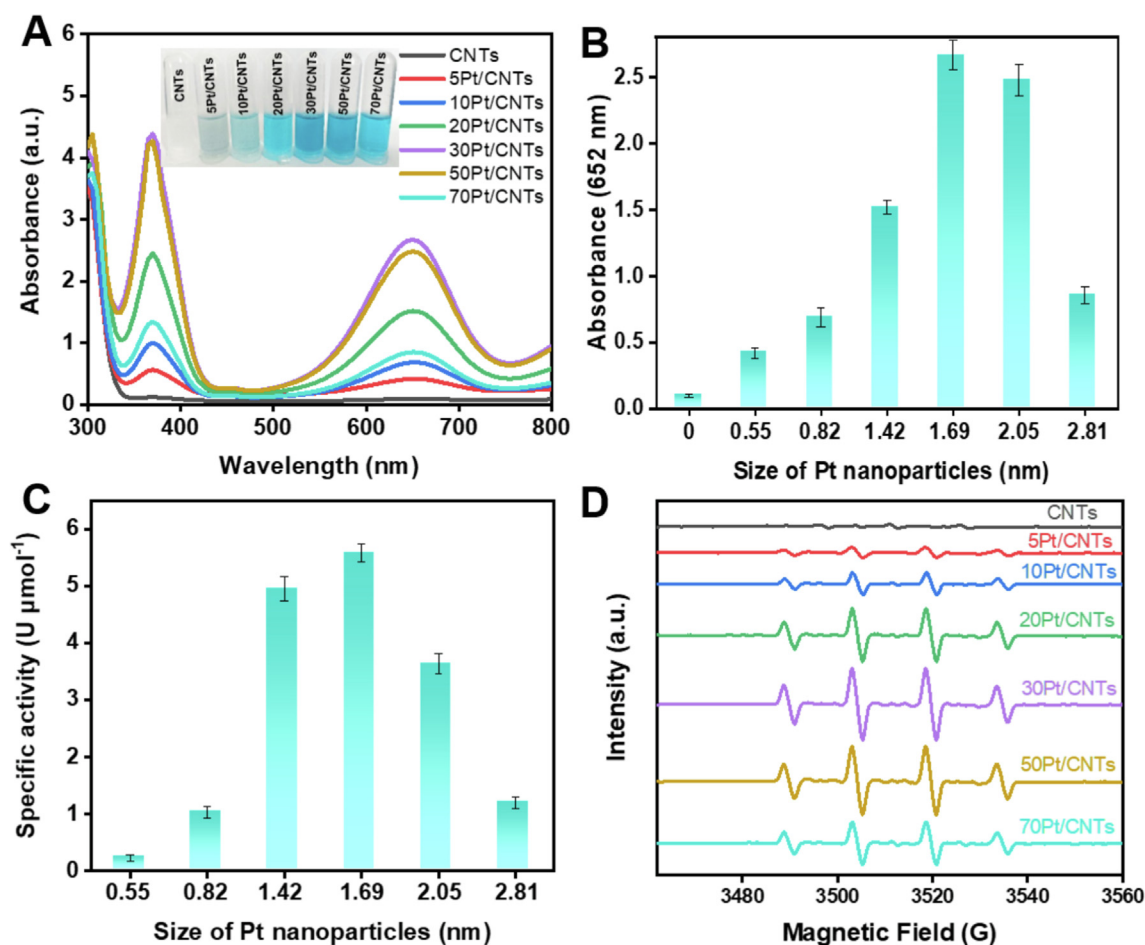


Fig. 2 POD-like property of the *c*Pt/CNTs nanozymes. (A) UV-vis spectroscopy of *c*Pt/CNTs ($c = 0, 5, 10, 20, 30, 50,$ and 70) nanozymes (the same molar amount of Pt). Inserted images (tubes) represent the visual color changes of TMB. (B) The absorption value of TMB at 652 nm compared to different sizes of Pt nanoparticles. (C) The SA of *c*Pt/CNTs nanozymes at 652 nm compared to different sizes of Pt nanoparticles. (D) DMPO spin-trapping ESR spectra of the ultrasmall TA-Ag nanozyme for H_2O_2 .

cles, as shown in Fig. 2C, it is found that the SA of *c*Pt/CNTs nanozymes also exhibits a volcanic relationship with the size of Pt nanoparticles, and the Pt particles with a size of 1.69 nm (30Pt/CNTs nanozyme) present the highest specific catalytic activity. To further verify the POD-like activity of *c*Pt/CNTs nanozymes, the generated $\bullet\text{OH}$ was detected by ESR spectroscopy (Fig. 2D). (Meng et al., 2022) The ESR signal intensity of $\bullet\text{OH}$ in *c*Pt/CNTs nanozymes also exhibits a volcanic relationship with the size of Pt nanoparticles, and the 30Pt/CNTs nanozyme present the highest intensity, confirming the presence of $\bullet\text{OH}$, which demonstrates that the Pt/CNTs nanozyme is an efficient POD-like catalyst. The above experimental results indicate that *c*Pt/CNTs nanozymes fabricated by ALD have a size-dependent activity in POD-like catalytic reaction, and the POD-like activity can be optimized by regulating the particle size of Pt by ALD.

3.3. Mechanistic and kinetic insights into size-dependent POD-like activity in Pt/CNTs nanozymes

The steady-state kinetic of oxidation of TMB with H_2O_2 was conducted for *c*Pt/CNTs ($c = 5, 10, 20, 30, 50,$ and 70) to determine the enzyme kinetic parameters to understand the

catalytic mechanism of size-dependent POD-like activity. (Jiang et al., 2018) Clearly, within the suitable range of TMB and H_2O_2 , typical Michaelis-Menten curves are received for Pt nanoparticles with the sizes of 0.55 nm, 0.82 nm, 1.42 nm, 1.69 nm, 2.05 nm, and 2.81 nm, respectively (Figs. 3 and 4). The data were fitted based on the Michaelis-Menten equation, and the enzymatic parameters were determined with the typical double-reciprocal Lineweaver-Burk plots (Inserted images in Figs. 3 and 4). (Lineweaver and Burk, 1934) The calculated enzyme kinetic parameters are listed in Table S3 and Table S4, which show that 5Pt/CNTs nanozyme displays a smaller K_m value for TMB and H_2O_2 , suggesting a higher affinity to substrates than other nanozyme. However, in a catalytic reaction, the reaction substrate is strongly adsorbed by the catalyst and will make it difficult to desorption later, which in turn will lead to a decrease in reactivity. (Chen et al., 2014) It can be seen from the TEM characterization that the size of Pt in 5Pt/CNTs is about 0.55 nm, which indicates that Pt is composed of small clusters of several Pt atoms. In general, this small size cluster has richer surface charge, which are beneficial to adsorb positively charged TMB, resulting in a high affinity. For the surface charge of 5Pt/CNTs, we can determine it by zeta potential. As shown in Figure S5, both CNTs and *c*Pt/

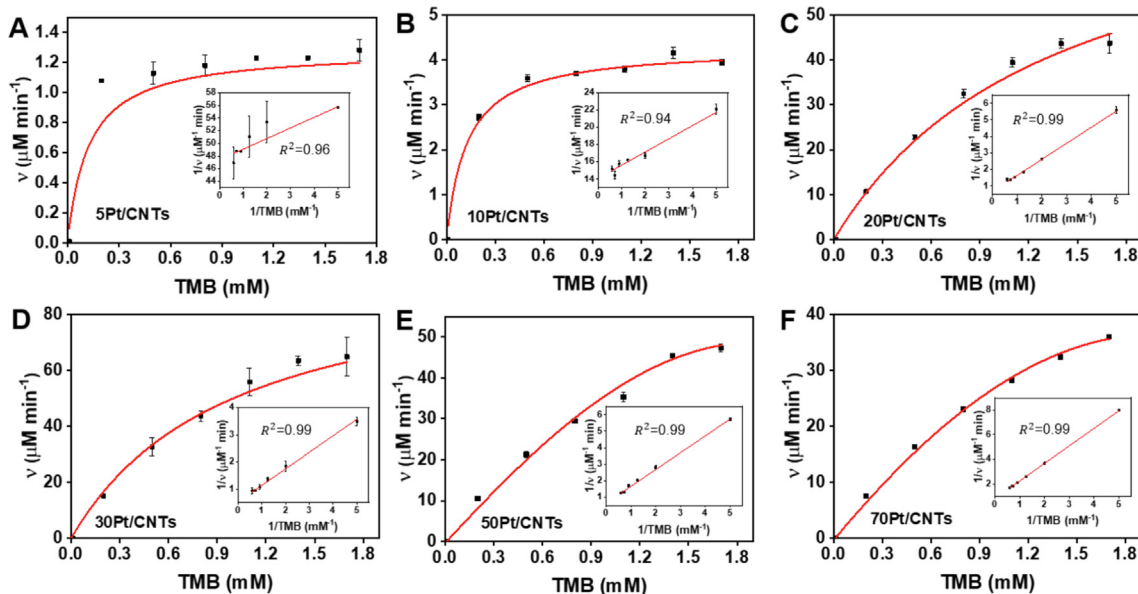


Fig. 3 Steady-state kinetics of the *c*Pt/CNTs nanozymes for TMB kinetic assay in the presence of H_2O_2 . (A-F) Michaelis-Menten curves for *c*Pt/CNTs nanozymes with varied TMB concentrations in the presence of H_2O_2 . Inserted images represent the Lineweaver-Burk plots of the double reciprocal of the Michaelis-Menten equation. Error bars shown represent standard errors derived from three independent experiments.

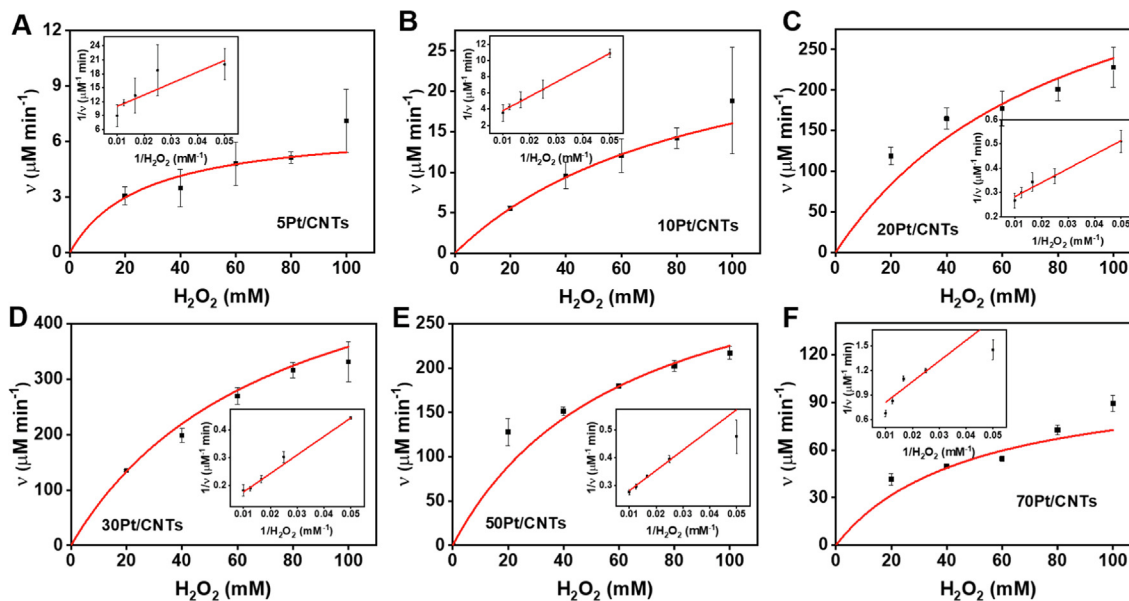


Fig. 4 Steady-state kinetics of the *c*Pt/CNTs nanozymes for H_2O_2 kinetic assay in the presence of TMB. (A-F) Michaelis-Menten curves for *c*Pt/CNTs nanozymes with varied H_2O_2 concentrations in the presence of TMB. Inserted images represent the Lineweaver-Burk plots of the double reciprocal of the Michaelis-Menten equation. Error bars shown represent standard errors derived from three independent experiments.

CNTs have negative surface zeta potentials, which is not only beneficial to the solubility and dispersibility of Pt/CNTs in water, but also beneficial to adsorb positively charged TMB. It is also found that 5Pt/CNTs has the largest negative surface zeta potential, indicating that it had the strongest adsorption effect on the reaction substrate, which is consistent with kinetic analysis. While K_m values for TMB and H_2O_2 display different trends of change with increasing the size from 0.55 nm to

2.81 nm. In contrast, v_{\max} and k_{cat} values for TMB and H_2O_2 show a volcanic trend and 30Pt/CNTs (1.69 nm) nanozyme has the largest v_{\max} and k_{cat} , indicating that 30Pt/CNTs exhibits the highest catalytic efficiency among these *c*Pt/CNTs nanozymes. For *c*Pt/CNTs ($c = 10, 20, 30, 50$ and 70), whose surface contains a small negative potential, has a proper adsorption/desorption effect on the reaction substrate, so they have better catalytic performance, of which 30Pt/CNTs have

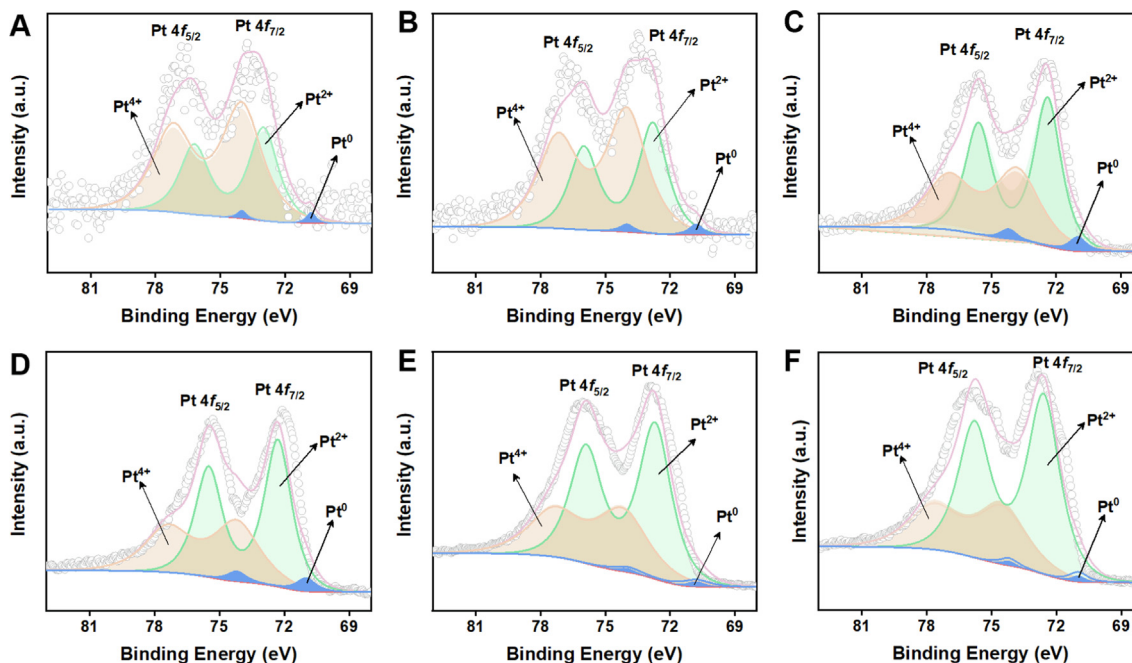


Fig. 5 High-resolution Pt 4f XPS of 5Pt/CNTs (A), 10Pt/CNTs (B), 20Pt/CNTs (C), 30Pt/CNTs (D), 50Pt/CNTs (E), and 70Pt/CNTs (F) nanozymes.

the best reactivity. Therefore, a proper adsorption of nanozymes with appropriate size on the substrates is more conducive to the catalytic activity. Moreover, it is obvious that this value is higher than that of reported Pt-based nanozymes (Table S3 and S4), demonstrating the excellent performance of 30Pt/CNTs fabricated by ALD.

To further reveal the catalytic mechanism of size-dependent POD-like activity, high-resolution Pt 4f XPS characterization was employed to probe the surface composition of Pt nanoparticles and the difference in the electronic properties of the *c*Pt/CNTs nanozymes. As shown in Fig. 5, the Pt 4f region exhibits doublets from the spin-orbit splitting of the 4f_{7/2} and 4f_{5/2} states, both of which can be deconvoluted into three peaks, indicating that all the *c*Pt/CNTs nanozymes consist of metallic Pt⁰, Pt²⁺, and Pt⁴⁺. (Gan et al., 2020) The existence of platinum oxide phases can be ascribed to the ultra-size of Pt nanoparticles, which are susceptible to oxidation by O₃ exposure during the ALD process or in the ambient environment. (Chen et al., 2014; Zhang et al., 2017) Meanwhile, the strength of the Pt 4f peak increase with Pt ALD cycle number (Figure S6), suggesting that the Pt content is gradually increasing, which is consistent with the above-mentioned ICP-AES and XPS surveys. According to literature, a high ratio of Pt⁰/Pt²⁺ in the surface composition of Pt nanoparticles is beneficial to improving the POD-like activity of Pt nanoparticles. (Chen et al., 2020) We calculated the ratios of Pt⁰/Pt²⁺; Pt⁰/Pt⁴⁺ and Pt²⁺/Pt⁴⁺ on the surface of *c*Pt/CNTs nanozymes. As shown in Table S5, the ratios of Pt⁰/Pt²⁺ and Pt⁰/Pt⁴⁺ exhibit a volcanic curve with the cycle number of Pt ALD increasing from 5 cycles (0.55 nm) to 70 cycles (2.81 nm), and the 30Pt/CNTs nanozyme with a size of 1.69 nm shows the maximum Pt⁰/Pt²⁺ and Pt⁰/Pt⁴⁺ values, which is consistent with the results of size-dependent POD-like activity. However, the ratio of Pt²⁺/Pt⁴⁺ tends to increase with the cycle number of Pt ALD. The above results demonstrate that Pt⁰ and Pt²⁺ species are the main catalytic reaction species, and

their content has a great influence on the catalytic activity. And Pt⁴⁺ species do have a certain impact on the activity of nanozymes, which is consistent with the result of literature. (Fu et al., 2014).

As reported in the literature, the POD-like reaction follows the Eley-Rideal mechanism: H₂O₂ molecules are initially adsorbed on the surface of Pt nanoparticles, and the Pt active site rapidly breaks the oxygen-oxygen bond of H₂O₂ to generate two surfaces •OH species (H₂O₂ → 2•OH), which are stabilized on the nanoparticles' surface via partial electron exchange interactions between the unpaired electrons of the adsorbed radicals and the conduction-band electrons of the metallic particles. Then, the surface •OH species can further oxidize the adsorbed TMB on the surface of Pt nanoparticles to form a blue color product. (Ge et al., 2018; Ma et al., n. d.; Ma et al., 2011) However, the adsorption of TMB and H₂O₂ should not be too strong, otherwise they will be hardly desorbed from the surface of Pt nanoparticles, which probably leads to nanozyme poisoning and inactivation. (Chen et al., 2021) To more clearly study the catalytic mechanism of size-dependent POD-like activity, based on the above results, we have proposed a correlation between the size of Pt nanoparticles and the ratio of Pt⁰/Pt²⁺ or POD-like activities (specific activity, *k*_{cat} of TMB and H₂O₂). As shown in Fig. 6, the ratio of Pt⁰/Pt²⁺ and specific activity, as well as *k*_{cat} of substrates, exhibit a volcanic relationship with the size of Pt nanoparticles, in which the 30Pt/CNTs nanozyme with a size of 1.69 nm gives rise to a higher catalytic efficiency owing to appropriate adsorption of the nanozyme on substrates.

3.4. Size-dependent antibacterial activity in Pt/CNTs nanozymes

POD-like nanozymes have been widely used in antibacterial application. It decomposes H₂O₂ into highly toxic free radicals

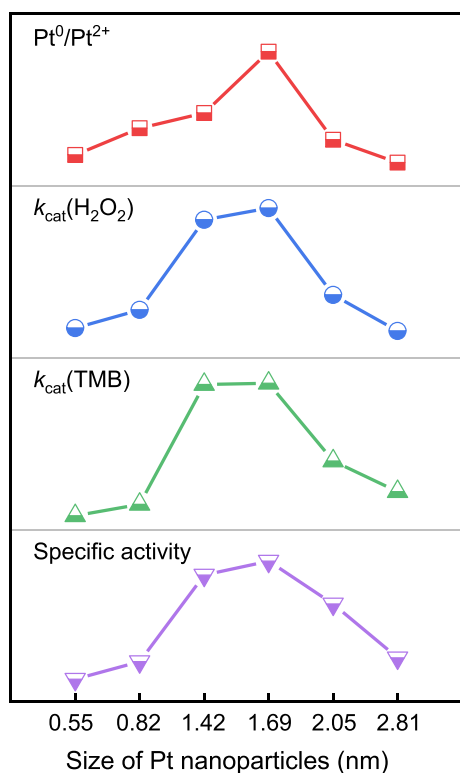


Fig. 6 Correlation between the size of Pt nanoparticles and ratio of $\text{Pt}^0/\text{Pt}^{2+}$ or POD-like activities (specific activity, k_{cat} of TMB and H_2O_2).

($\bullet\text{OH}$, Fig. 2D), thereby destroying bacterial membrane and induce apoptosis. (Chen et al., 2021; Sun et al., 2020) Based on the size-dependent POD-like activity of *cPt/CNTs* nanozymes, we evaluated the broad-spectrum antimicrobial capability of *cPt/CNTs* nanozymes against Gram-negative *E. coli*

and Gram-positive *S. aureus*. As shown in Fig. 7A and 7C, *cPt/CNTs* nanozymes in the absence of H_2O_2 showed negligible killing effect against *E. coli* and *S. aureus*. In the presence of H_2O_2 (0.2 mM), the viability of both *E. coli* and *S. aureus* decreases effectively, indicating the antibacterial activity of *cPt/CNTs* nanozymes employ their POD-like catalytic activity to decompose H_2O_2 into highly toxic $\bullet\text{OH}$ that disrupt the bacterial membrane and induce bacterial apoptosis. (Mei et al., 2021) In comparison, the 30Pt/CNTs nanozyme with a size of 1.69 nm exhibits a much higher antibacterial activity than other *cPt/CNTs* nanozymes under the same experimental conditions. The plate counting method was employed to quantify the antibacterial activity of *cPt/CNTs* nanozymes. As shown in Fig. 7B and 7D, the antibacterial activity of *cPt/CNTs* nanozymes exhibits a volcanic relationship with Pt ALD cycle number, in which 30Pt/CNTs nanozymes presented the highest antibacterial activity against *E. coli* (~81 %) and *S. aureus* (~54 %). In order to fully characterize the antibacterial properties of *cPt/CNTs* nanozymes, we carried out the inhibition zone experiment. (Xia et al., 2018; Yang et al., 2019) The antibacterial performance of all the samples was displayed in Figure S7. Notably, after incubation for about 24 h, the as-prepared *cPt/CNTs* nanozymes presents the robust antibacterial activity, comparing with that of bare CNTs samples. And the antibacterial activity of *cPt/CNTs* nanozymes exhibits a volcanic relationship with Pt ALD cycle number, in which 30Pt/CNTs nanozymes presented the highest antibacterial activity against *E. coli* (3.8 cm) and *S. aureus* (3.17 cm). It is also noticeable that *E. coli* was more sensitive toward antibacterial treatments as reported in the literature, (Yin et al., 2016; Liu et al., 2021; Xue et al., 2022) which could be ascribed to the difference in their membrane structure. (Gupta et al., 2019) And, we compared with the antibacterial properties of relevant nanozymes in the literature and found that the antibacterial properties of Pt/CNTs nanozymes are very close to or even higher than those of Pt-based nanozymes, demonstrating the superiority of ALD technique. (Ge et al., 2018; Chen et al.,

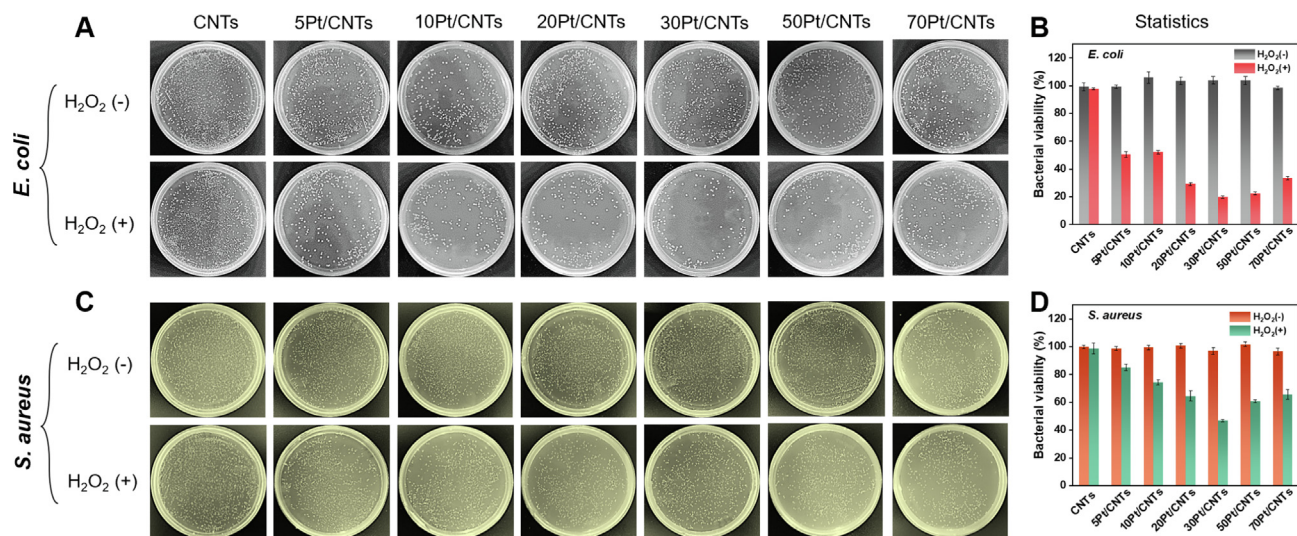


Fig. 7 Antibacterial properties of the *cPt/CNTs* nanozymes. Photographs of bacterial colonies formed by (A) *E. coli* and (C) *S. aureus* treated with *cPt/CNTs* nanozymes with or without H_2O_2 . The plate counting method determines the corresponding bacterial viabilities of (B) *E. coli* and (D) *S. aureus* after treatment with *cPt/CNTs* nanozymes in different groups. Error bars shown represent standard errors derived from three independent experiments.

2021) The above experimental results indicate that the cPt/CNTs nanozymes have a size-dependent antibacterial activity, consistent with the POD-like activity of the cPt/CNTs nanozymes. Meanwhile, the optimization of the antibacterial activity can be realized by controlling Pt nanoparticle size by ALD.

H₂O₂ is a common fungicide in clinic, which can destroy bacterial cell membrane, protein and nucleic acid. (Kalyanaraman, 2013) However, in the clinic, due to the high concentration of H₂O₂ (2 M) required and poor antibacterial properties, it is easy to develop drug resistance. (Djorić and Christopher, n.d.) The results unveil that a low content of 30Pt/CNTs nanozyme (0.2 mg/mL) could kill ≥ 80 % of *E. coli* in the presence of extremely low concentrations of H₂O₂ (0.2 mM), while the bactericidal efficiency of bare CNTs was negligible. (Fig. 7A and 7C) Therefore, the development of nanozyme-based high-performance fungicides provides a new strategy to address bacterial infection and drug resistance.

4. Conclusion

In summary, we have successfully implemented a general method based on ALD to optimize the POD-like activity and antibacterial properties of Pt-based nanozymes by tuning Pt ALD cycle number. Among all the nanozymes, the as-prepared 30Pt/CNTs nanozymes with a size of 1.69 nm exhibit much higher POD-like activity and antibacterial properties than other cPt/CNTs nanozymes. A combination of kinetic and XPS analyses as well as multiple nanozyme characterizations revealed that relatively reasonable adsorption of the nanozymes with an appropriate size on the substrates contributes to efficient catalytic activity, which give rise to size-dependent activity in the reaction. A volcanic relationship between the size of Pt nanoparticles and the ratio of Pt⁰/Pt²⁺, POD-like activities or antibacterial activity was proposed for cPt/CNTs nanozymes. These results demonstrate that Pt nanoparticle size plays a crucial role in the design and optimization of active nanozymes for POD-like reaction and antibacterial performance. This work presents that regulating the particle size of nanozymes by ALD is an effective strategy to regulate the enzymatic performance, and provides insight for an in-depth understanding catalytic mechanism of nanozymes during antibacterial processes.

Declaration of Competing Interest

The authors declare that they have no known competing financial interests or personal relationships that could have appeared to influence the work reported in this paper.

Acknowledgements

This work has been financially supported by the National Natural Science Foundation of China, China (8211001138, 82071987, 81771907, 82001962, U1910209), Research Project Supported by Shanxi Scholarship Council of China, China (2020-177), Fund Program for the Scientific Activities of Selected Returned Overseas Professionals in Shanxi Province, China (20200006), Four Batches of Scientific Research Projects of Shanxi Provincial Health Commission (2020TD11, 2020SYS15, 2020XM10), Key Laboratory of Nano-imaging and Drug-loaded Preparation of Shanxi Province, China (202104010910010), Shanxi Province Science Foundation for Youths, China (202103021223406, 20210302124128), Scientific and Technological Innovation Programs of Higher Education Institutions in Shanxi, China (2021L200), China Postdoctoral Science Foundation, China (2021T140432, 2019M661056).

Appendix A. Supplementary material

Supplementary data to this article can be found online at <https://doi.org/10.1016/j.arabjc.2022.104238>.

References

- Bell; Alexis; T. *Science* **2003**
- Chen, M.S., Cai, Y., Yan, Z., Gath, K.K., Axnanda, S., Goodman, D. W., 2007. *Surf. Sci.* 601 (23), 5326–5331.
- Chen, W., Ji, J., Feng, X., Duan, X., Qian, G., Li, P., Zhou, X., Chen, D., Yuan, W., 2014. *J. Am. Chem. Soc.* 136 (48), 16736–16739.
- Chen, Y., Yuchi, Q., Li, T., Yang, G., Miao, J., Huang, C., Liu, J., Li, A., Qin, Y., Zhang, L., 2020. *Sens. Actuators, B* 305, 127436.
- Chen, Y., Wang, P., Hao, H., Hong, J., Li, H., Ji, S., Li, A., Gao, R., Dong, J., Han, X., Liang, M., Wang, D., Li, Y., 2021. *J. Am. Chem. Soc.* 143 (44), 18643–18651.
- den Breejen, J.P., Radstake, P.B., Bezemer, G.L., Bitter, J.H., Frøseth, V., Holmen, A., de Jong, K.P., 2009. *J. Am. Chem. Soc.* 131 (20), 7197–7203.
- Djorić, D.; Kristich Christopher, J. *Antimicrobial Agents and Chemotherapy* 59, (1), 159–169.
- Fu, Y., Zhao, X., Zhang, J., Li, W., 2014. *J. Phys. Chem. C* 118 (31), 18116–18125.
- Gan, J., Zhang, J., Zhang, B., Chen, W., Niu, D., Qin, Y., Duan, X., Zhou, X., 2020. *J. Energy Chem.* 45, 59–66.
- Ge, C., Wu, R., Chong, Y., Fang, G., Jiang, X., Pan, Y., Chen, C., Yin, J.-J., 2018. *Adv. Funct. Mater.* 28 (28), 1801484.
- Gupta, A., Mumtaz, S., Li, C.-H., Hussain, I., Rotello, V.M., 2019. *Chem. Soc. Rev.* 48 (2), 415–427.
- Jiang, B., Duan, D., Gao, L., Zhou, M., Fan, K., Tang, Y., Xi, J., Bi, Y., Tong, Z., Gao, G.F., Xie, N., Tang, A., Nie, G., Liang, M., Yan, X., 2018. *Nat. Protoc.* 13 (7), 1506–1520.
- Jiang, D., Ni, D., Rosenkrans, Z.T., Huang, P., Yan, X., Cai, W., 2019. *Chem. Soc. Rev.* 48 (14), 3683–3704.
- Kalyanaraman, B., 2013. *Redox Biol.* 1 (1), 244–257.
- Li, Z., Wang, Z., Qiu, X., Bai, L., Zheng, J., 2018. *J. Therm. Anal. Calorim.* 133 (3), 1353–1364.
- Li, Z.-Y., Xia, Y., 2010. *Nano Lett.* 10 (1), 243–249.
- Li, X., Yang, X., Cheng, X., Zhao, Y., Luo, W., Elzatahry, A.A., Alghamdi, A., He, X., Su, J., Deng, Y., 2020. *J. Colloid Interface Sci.* 570, 300–311.
- Liang, M., Yan, X., 2019. *Acc. Chem. Res.* 52 (8), 2190–2200.
- Lineweaver, H., Burk, D., 1934. *J. Am. Chem. Soc.* 56 (3), 658–666.
- Liu, L., Du, B., Shang, C., Wang, J., Wang, E., 2018. *Anal. Chim. Acta* 1014, 77–84.
- Liu, Z., Zhao, X., Yu, B., Zhao, N., Zhang, C., Xu, F.-J., 2021. *ACS Nano* 15 (4), 7482–7490.
- Ma, C.-B.; Xu, Y.; Wu, L.; Wang, Q.; Zheng, J.-J.; Ren, G.; Wang, X.; Gao, X.; Zhou, M.; Wang, M.; Wei, H. *Angewandte Chemie International Edition*, (e202116170).
- Ma, M., Zhang, Y., Gu, N., 2011. *Colloids Surf. A: Physicochem. Eng. Asp.* 373 (1), 6–10.
- Mayrhofer, K.J.J., Blizanac, B.B., Arenz, M., Stamenkovic, V.R., Ross, P.N., Markovic, N.M., 2005. *J. Phys. Chem. B* 109 (30), 14433–14440.
- Mei, L., Zhu, S., Liu, Y., Yin, W., Gu, Z., Zhao, Y., 2021. *Chem. Eng. J.* 418, 129431.
- Meng, F.; Peng, M.; Chen, Y.; Cai, X.; Huang, F.; Yang, L.; Liu, X.; Li, T.; Wen, X.; Wang, N.; Xiao, D.; Jiang, H.; Xia, L.; Liu, H.; Ma, D. *Applied Catalysis B: Environmental* **2022**, 301
- Moglianetti, M., De Luca, E., Pedone, D., Marotta, R., Catelani, T., Sartori, B., Amenitsch, H., Retta, S.F., Pompa, P.P., 2016. *Nanoscale* 8 (6), 3739–3752.
- Ramachandran, R.K., Dendooven, J., Filez, M., Galvita, V.V., Poelman, H., Solano, E., Minjauw, M.M., Devloo-Casier, K.,

- Fonda, Hermida-Merino, D., Bras, W., Marin, G.B., Detavernier, C., . ACS Nano 10 (9), 8770–8777.
- Sanchez, A., Abbet, S., Heiz, U., Schneider, W.D., Häkkinen, H., Barnett, R.N., Landman, U., 1999. J. Phys. Chem. A 103 (48), 9573–9578.
- Sun, D., Pang, X., Cheng, Y., Ming, J., Xiang, S., Zhang, C., Lv, P., Chu, C., Chen, X., Liu, G., Zheng, N., 2020. ACS Nano 14 (2), 2063–2076.
- Wang, H., Wan, K., Shi, X., 2019. Adv. Mater. 31 (45), 1805368.
- Wang, H., Gu, X.-K., Zheng, X., Pan, H., Zhu, J., Chen, S., Cao, L., Li, W.-X., Lu, J., 2019. Sci. Adv. 5 (1), eaat6413.
- Wang, Z., Zhang, R., Yan, X., Fan, K., 2020. Mater. Today 41, 81–119.
- Wei, F., Cui, X., Wang, Z., Dong, C., Li, J., Han, X., 2021. Chem. Eng. J. 408, 127240.
- Weng, Y., Chen, X., Chen, H., Yang, H., Gong, Z., Tan, H., 2022. Chem. Eng. J. 442, 136153.
- Wilson, O.M., Knecht, M.R., Garcia-Martinez, J.C., Crooks, R.M., 2006. J. Am. Chem. Soc. 128 (14), 4510–4511.
- Xia, L., Xu, M., Cheng, G., Yang, L., Guo, Y., Li, D., Fang, D., Zhang, Q., Liu, H., 2018. Carbon 130, 775–781.
- Xing, S., Gao, Z., Lv, Z., Zhao, S., Xiong, M., Zhang, J., Wang, G., Qin, Y., 2022. Carbon 188, 385–392.
- Xue, H.; Meng, A.; Yang, T.; Li, Z.; Chen, C. *Journal of Energy Chemistry* **2022**.
- Yang, J., Fu, W., Chen, C., Chen, W., Huang, W., Yang, R., Kong, Q., Zhang, B., Zhao, J., Chen, C., Luo, J., Yang, F., Duan, X., Jiang, Z., Qin, Y., 2021. ACS Catal. 11 (7), 4146–4156.
- Yang, L., Meng, F., Qu, X., Xia, L., Huang, F., Qin, S., Zhang, M., Xu, F., Sun, L., Liu, H., 2019. Carbon 155, 397–402.
- Yin, W., Yu, J., Lv, F., Yan, L., Zheng, L.R., Gu, Z., Zhao, Y., 2016. ACS Nano 10 (12), 11000–11011.
- Zhang, J., Chen, C., Chen, S., Hu, Q., Gao, Z., Li, Y., Qin, Y., 2017. Catal. Sci. Technol. 7 (2), 322–329.
- Zhang, B., Chen, C., Liu, J., Qiao, W., Zhao, J., Yang, J., Yu, Y., Chen, S., Qin, Y., 2020. Appl. Surf. Sci. 508, 144869.
- Zhang, J., Gao, Z., Wang, S., Wang, G., Gao, X., Zhang, B., Xing, S., Zhao, S., Qin, Y., 2019. Nat. Commun. 10 (1), 4166.
- Zhang, B., Qin, Y., 2018. ACS Catal. 8 (11), 10064–10081.
- Zhao, S., Yang, J., Duan, F., Zhang, B., Liu, Y., Zhang, B., Chen, C., Qin, Y., 2021. J. Colloid Interface Sci. 598, 45–55.